PRESIOUS

Predictive digitization, restoration and degradation assessment of cultural heritage objects

D3.6 – Degradation Prediction Methodology Report

Grant Agreement Number	600533
Project Acronym	PRESIOUS
Project Title	PREdictive digitization, reStoration and degradatIOn assessment of cultUral heritage objectS
Funding Scheme	Collaborative Project (STREP)
Name, title and organisation of the scientific representative of the project's coordinator	T. Theoharis, Professor, NTNU
Telephone	+47 73591447
Email	theotheo@idi.ntnu.no
Project Website Address	www.presious.eu
Dissemination Level	PU

Address
O. S. Bragstads plass 2 E
Gløshaugen, NTNU, NO-7491 Trondheim,
Norway

http://presious.eu

Contact person
Karelle Gilbert-Soni
karelle@ime.ntnu.no
+ 47 73591481

Deliverable Identification Sheet

Grant Agreement number	600533
Project Acronym	PRESIOUS
Project Title	PREdictive digitization, reStoration and degradatIOn assessment of cultUral heritage objectS
Funding Scheme	Collaborative Project (STREP)
Contractual Delivery Date	M30
Deliverable Number	D3.6
Deliverable Name	Degradation Prediction – Methodology Report
Type	Document (LaTeX)
Deliverable Version	1.0
Status	Final
Associated WP / Task	WP3
Author(s)	Christian Schellewald, Panagiotis Perakis, Theoharis Theoharis, Konstantinos Sfikas, Kidane Fanta
Other Contributors	G. Stamatelatos, K. Zagoris
Project Officer	Philippe Gelin
Abstract	This document contains the methodology report for the stone erosion simulator.
Circulated to Participants	25. September, 2015
Read by Participants	25. September, 2015
Approved by General Assembly	30. September, 2015

Document Revision History

Date	Version	Author/Editor/Contributor	Summary of Changes
05.07.2015	0.1	Christian Schellewald	Very first version
19.07.2015	0.4	Panagiotis Perakis	Structure for the Erosion simulator report
15.09.2015	0.7	Panagiotis Perakis	Merged Methodology Report Erosion simulator
20.09.2015	0.9	Christian Schellewald	Methodology Report 2D Stone-texture sampling
25.09.2015	0.95	Panagiotis Perakis	Minor corrections incorporated
29.09.2015	1.0	Christian Schellewald	Final Version

Contents

1 Introduction

The computer simulation of the naturally occurring stone degradation process is very attractive because it could enable us to predict the future state of important Cultural Heritage (CH) monuments based on different environment scenarios and thus allow us to take appropriate action in good time. The purpose of this study is to contribute to the simulation of the fundamental and most common degradation mechanisms that impact objects that are built out of stone. Our ultimate aim is to model and simulate the physico-chemical processes that lead to the degradation of the stone-material of CH objects over time. Towards this aim we are implementing a prototype software application that simulates surface mesh alterations of CH objects and allows therefore to imitate manifestations of stone degradation phenomena like surface recession and crust formation.

The three main degradation processes which often work simultaneously to decompose rocks are *physical/mechanical*, *chemical* and *biological* in nature. One of the main causes of stone decay is the interaction between water and the porous structure. Water absorption can induce weathering on stone materials in several ways:

1. by **chemical reaction** with industrial pollutants mainly the atmospheric gases of carbon dioxide CO_2, sulfur dioxide SO_2 and nitrogen dioxide NO_2, that decay the stone material by changing its chemical composition;
2. by a physical mechanism through **mechanical stresses** due to freeze/thaw and wet/dry cycles, that disintegrate stones into smaller particles, which then can be removed by gravity, wind, water or ice;
3. by acting as a transport medium for **salts** in dissolution and recrystallization processes within the pore space;
4. by providing an essential substrate for **biological growth** of living organisms such as bacteria, fungi, algae and lichens.

Stone decay appears in many different forms. Stone may gradually and slowly weather away, leaving a solid surface behind. At other times sheets or flakes break off from the stone at once. Sometimes the surface starts to show blisters or a stone just loses its integrity and crumbles away. Some of the stones can appear perfectly intact for a long time while already losing cohesion underneath.

The two different chemical weathering scenarios that are usually distinguished are the weathering within a natural environment and the weathering within a polluted environment. The first (unpolluted) scenario considers (beside the air) only the gas carbon dioxide (CO_2) while the second scenario contains also the industrial gases sulfur and nitrogen dioxide (SO_2 and NO_2). The chemical weathering results in two main effects; the gain or loss of material. The first one is mostly visible as

crust building up on surfaces while the second one relates in most cases to surface recession. The crust formation is usually due to the deposition of chemical material in polluted environments while the loss of material results mainly due to reactions of water with the stone-material and pollution gases. The chemical products in this process are subsequently washed away. Temperature and humidity play crucial roles in these processes.

The two different mechanical weathering scenarios that are usually distinguished are the weathering caused by soluble salts and the weathering caused by wet/dry and freeze/thaw cycles. Along with air pollution, soluble salts represent one of the most important causes of stone decay. Salts cause damage to stone in several ways. The most important is the growth of salt crystals within the pores, fissures and cracks of a stone, which can generate stresses that are sufficient to overcome the stone's tensile strength and turn the stone to fragmented pieces. Another important decay mechanism under the general term "differential stress" includes the effects of wet/dry cycling, clay swelling, differential hygric stress, differential thermal stress, and stress from differential expansion rates of material in pores (such as salts or organic material) versus in the stone [3].

The small amount of recession rates observed at cultural heritage sites, the complexity of the deterioration mechanisms, the unavailability of chemical data that characterize the monument building materials on site, and the uncontrolled environmental conditions, make it necessary to setup accelerated erosion chambers for conducting specific purpose experiments, under controlled conditions using chemically characterized stone samples.

2 Object Degradation Prediction Methodology

2.1 Degradation Modules

The overall aim of the "Object Degradation Prediction" module is the estimation and prediction of monument degradation based on present-time surface shape and material measurements along with measurements of the environmental data. We subdivided the module into three components, namely the *Erosion Simulator*, the *Stone Builder* and the *Differential Geometry Measurer* (Fig. 1).

The core component of our "Object Degradation Prediction" module is the *Erosion Simulator*, which simulates the erosion process on the surface of an input mesh of a stone object. An important supplier module for the erosion simulation is the *Stone Builder* which is used to synthetically generate a specific type of stone. It is used either to fill in plausible stone data that fits a given or measured stone sample or to synthesize stone data from scratch for a specific stone type. The last component, the *Differential Geometry Measurer* (DGM), is an auxiliary and currently a more

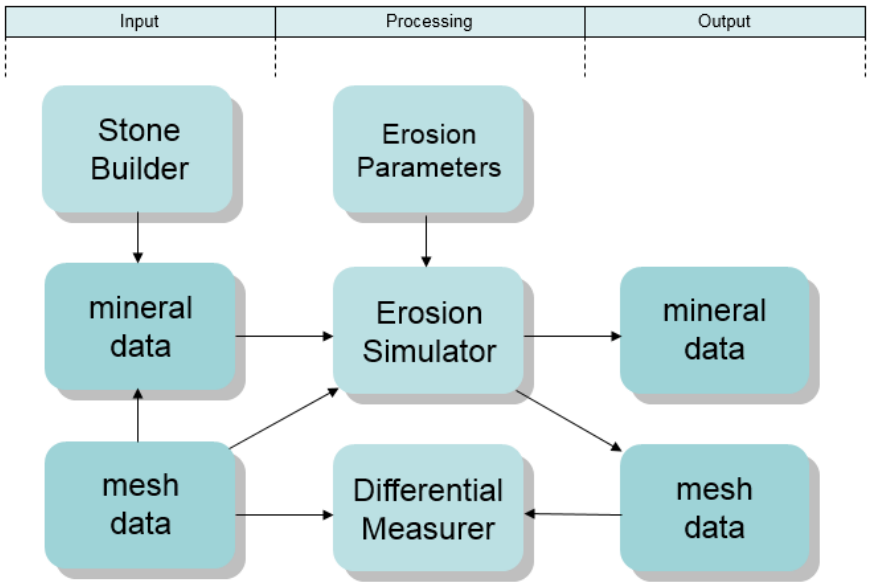

Figure 1: Pipeline of the "Degradation Prediction" module.

independent module that allows to align subsequent scans of the same stone surface and measures the difference (erosion) between them. Its basic purpose is to provide the ground-truth measurement from scanned eroded surfaces and will support the optimal adjustment of parameters that can be varied within the Erosion Simulator. Figure 1 shows the interactions of the three components and illustrates the basic data processing pipeline.

For each of the three components we describe the implemented methods along with some background information if necessary.

Current State

In order to provide an overview we list the current state of the implemented software components:

- **Stone Builder:** Prototypical implementation of a basic 2D texture synthesis approach on arbitrary connected surface meshes using 2D textures as input data.
  - Implementation of a locally defined coordinate system that is subsequently distributed to neighboring vertices in a consistent manner exploiting a Gram-Schmidt orthogonalization.
  - The local 3D vertices of the meshes are projected onto a flat surface perpendicular to the normal orientation.
  - The irregular flat mesh is projected onto a regular pixel-grid allowing to represent the neighborhood as a regular pixel-template for the sampling.

  - Mesh vertices are visited/traversed in breadth-first order and the sample value (i.e. the material) is determined by the already sampled neighborhood.
  - The mineral data that is exploited for the sampling procedure is a color-coded texture of the QEMSCANs of real stones.

- **Erosion Simulator:** Prototypical implementation of a mesh off-setting model that simulates the chemical degradation processes that occur on a homogeneous stone surface. Gauri's model for the erosion on marble has been adopted, implemented and extended to cover, in addition to homogeneous stones, stones that have a registered 3D mesh surface and QEMSCAN mineral data as texture.
  - Implementation of the erosion model as a combination of an mesh off-setting process (geometric model) using as an offset value the recession predicted by the Gauri erosion model (chemical model);
  - Implementation of the above erosion model for application to the whole mesh, considering homogeneous stones;
  - Implementation of a surface regular re-sampling algorithm for u,v mapping of the irregular stone slab surfaces;
  - Implementation of a registration procedure between the geometric mesh data and the QEMSCAN mineral data;
  - Implementation of the above erosion model for application to the stone surface talking into account not only the geometry but also the registered QEMSCAN mineral data as texture;

- **Differential Geometry Measurer:** Implementation of a module that aligns stone surface areas that are scanned consecutively at the cultural heritage sites or exposed to accelerated erosion and measures the erosion between two stone surface meshes scanned or computed.
  - Exploration and implementation of the Iterative Closest Point (ICP) algorithm and its variants on a Linux operating system. For our purposes also the commercial Windows software OPTOCAT from Breuckmann/Aicon is a suitable tool for registering and aligning slightly eroded stone surface areas .
  - Implementation of a mesh-to-mesh distance measurer for measuring mesh differences among model predictions or actual experimental data sets;

In the following sections we describe the background and the methodology that we explored towards the measurement and modeling of the stone degradation process. We start in Section 3 with the Stone-Builder that aims at a sampling of stone-material from given sparse measurements or from scratch. In Section 4 we are concerned with the the Erosion Simulator and the modeling of stone degradation process and its application to surface geometric and physico-chemical data. Section 5 describes the implementation of the Differential Geometry Measurer module. Finally, Section 6 summarizes the used ideas, the challenges and some concluding remarks.

3 The Stone Builder

Below we outline the stone building approach that we implemented with the aim of synthesizing stone-material for the degradation simulation. In particular we explain our approach to synthesize 2D stone-material from 2D stone-textures. One of our goals/constraints of the developed surface sampling method is to preserve the original mesh. The main purpose of the Stone Builder in its current version is the virtual synthesis of (realistic) surface stone-material. The resulting textured mesh can be subsequently used within the Erosion Simulator for the degradation simulation.

3.1 Surface Sampling On Regular Grids

For generating 2D textural images we decided (after exploring a few methods) to exploit non-parametric sampling methods for the creation of the stone textures on the meshes. However, in its basic version the underlying image grid structure of the involved textures and images are usually rectangular regular grids. In our case the example texture is on a rectangular regular grid as well but the mesh of the objects can be irregular. To cope with this difference we map the irregular grid locally onto a regular grid which makes it possible to transfer non-parametric sampling methods to our case. We explain this approach more detailed in section 3.2. Below we first outline the key ideas of non-parametric sampling methods which represent variants of Markov Random Field sampling methods.

3.1.1 2D Texture Markov Random Field Sampling

A mathematically well formulated texture synthesis approach is based on Markov Random Fields (MRFs) and exploits Gibbs sampling for the synthesis. Within this model a texture is interpreted as a local and stationary random process. However, an explicit probability function has to be modeled. Then sampling from this distribution results in a synthesized version of the texture, but unfortunately this approach is known to be computationally expensive. Therefore practical approaches resort to algorithms known as non-parametric sampling approaches. These were introduced for 2D textures by Efros and Leung [4] and we summarize the idea in the following section.

3.1.2 Efros & Leung's Algorithm

The main idea of the non-parametric sampling from Efros and Leung [4] is to use an example texture as a statistical model for Markov-random-field sampling. This allows to synthesize new texture samples from a given texture example. The main assumption is that the present example is large enough to capture the (statistical) properties of the texture even if the given sample is only a single draw out of an

(nearly) infinite number of possible samples. The texture is grown from a seed by sampling from the approximate conditional probability distribution:

$$P(x_{i,j}|N(x_{i,j}))$$

Here $N(x_{i,j})$ denotes the neighborhood of the pixel $x_{i,j}$ and $P(x_{i,j}|N(x_{i,j}))$ refers to the conditional probability distribution for the gray-values at location (i, j) when its neighborhood is determined. This model represents a Markov random field when the conditional probability depends only on the local neighborhood.

In its basic version the texture is synthesized starting from a seed pixel and then growing outwards. For the pixel $x_{i,j}$ that will be synthesized an approximation to the conditional probability $P(x_{i,j}|N(x_{i,j}))$ is obtained by weighting the candidates that fit best to the neighborhood $N(x_{i,j})$ of already synthesized pixels in the input texture. In practice one builds a template of already sampled neighborhood pixels and searches for the best candidate locations where the template fits best. The synthesized pixel value is obtained by sampling from the weighted best candidate pixels. Extensions to a multiresolution synthesis pyramid and a fixed neighborhood [12] lead to computationally effective variations and improvements of the approach. Exploiting a reference implementation by Paget [8] we illustrate in figure 2 the capability of synthesizing a 2D stone pattern from a 200x200 training patch taken from an electron microscopy image. The 2D approach captures the characteristics of the training texture and with increasing neighborhood and training texture size the long range characteristics – present in the electron microscopy image – become apparent. The 2D behavior of the non-parametric sampling approaches encouraged our development of a prototypical implementation of a new approach that allows the sampling of stone material on irregular mesh vertices based on 2D texture examples. We explain the ideas of this algorithm in the next section.

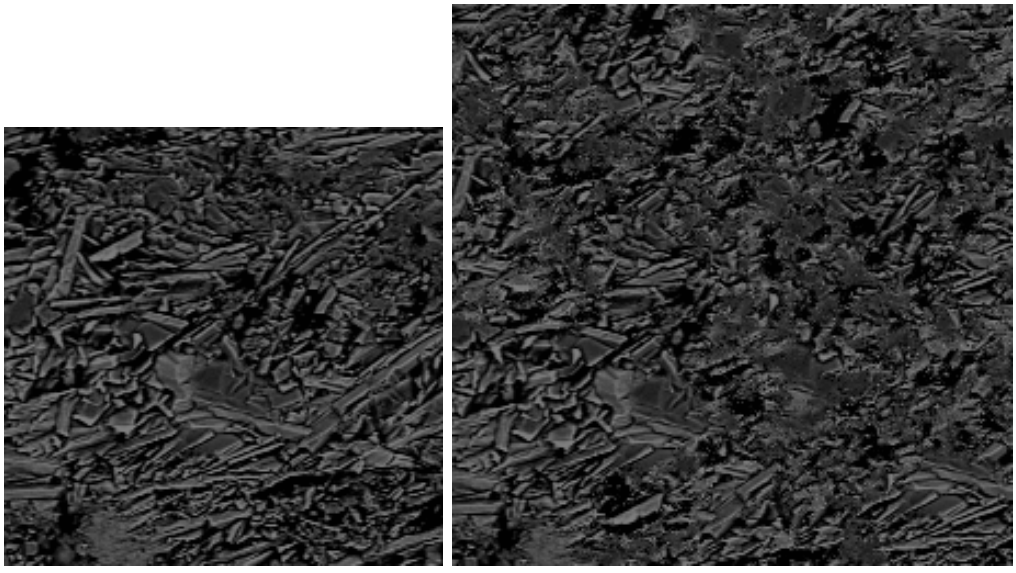

Figure 2: Non-parametric sampling approach. **Left:** A 200x200 pixel stone texture used as training example. **Right:** The synthesized 256x256 pixel large texture captures also the long range characteristics present within the stone texture example.

3.2 The Texture Generation Process

The main differences that appear when one tries to synthesize a texture onto an irregular 3D mesh-surface instead of a regular flat image grid are that there is no predefined orientation (in digital images the x- and y-axis are naturally horizontal and vertical aligned) and that the neighborhood vertices are irregular distributed (in images neighbor pixels are on a grid). This makes it more difficult to search for the best fitting candidate locations in the example texture and makes it difficult to handle non-homogeneous (=oriented) textures. We cope with this issues by assigning a locally defined orientation and map the irregular vertices during the sampling onto a regular pixel grid. We illustrate how we determine a local coordinate system for each vertex that is consistent/similar to neighboring vertices in the next section. Then we outline how the irregular neighbor vertices are mapped onto a regular template grid.

3.2.1 Local Coordinates

We create and distribute a locally defined orientation onto the full mesh by the following procedure. Starting from an arbitrary vertex the vertices of the mesh are visited/traversed in breadth-first order. For the starting vertex the normal vector is computed based on it's neighborhood vertices and defines the z-axis of the locally assigned coordinate system. For the first vertex the x- and y-axis might be selected arbitrary but should be orthogonal to the z-axis and to each other. This can for example be done by taking two different edges connected to the vertex as initial axis-candidates and orthonormalising them by a Gram-Schmidt process (see section 3.2.2). The current local coordinate system is then copied as approximation to the vertices in the neighborhood. When these neighborhood vertices are visited, the approximated z-axis is corrected/substituted by computing the accurate local normal vector based on the current neighborhood vertices. Subsequently the x- and y-axis are adapted to be orthonormal to the new normal vector by Gram-Schmidt steps. In this way the local coordinate system is spread to the neighborhood in a locally consistent way. Figure 3 illustrates the 2D positions of the vertices of a sphere-mesh when the local coordinate system is distributed from one seed onto the whole connected mesh.

3.2.2 Gram-Schmidt Orthonormalising

One key step when we define and distribute the locally defined coordinate system is the Gram-Schmidt orthogonalization. We consider the three dimensional case ($N = 3$) but this easily transfers to arbitrary dimensions. When we define the orthogonal projection of the vector $\mathbf{v} \in \mathbb{R}^N$ onto a vector $\mathbf{u} \in \mathbb{R}^N$as

$$\mathrm{proj}_{\mathbf{u}}(\mathbf{v}) = \frac{\mathbf{v}^T\mathbf{u}}{\mathbf{u}^T\mathbf{u}}\mathbf{u}$$

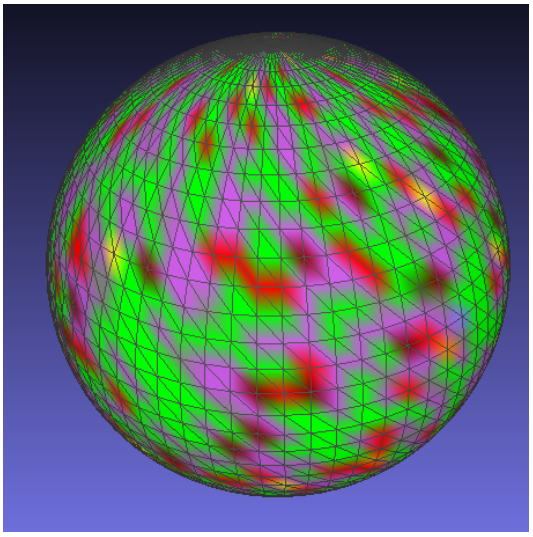

Mesh of a 3D sphere (91 vertices)

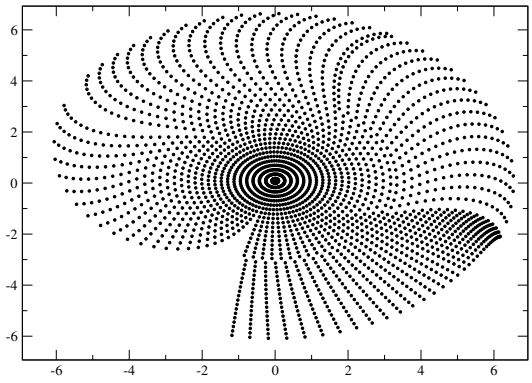

2D positions of the vertices when distributing a (seed based) local coordinate system onto the whole mesh.

Figure 3: Illustration of the local coordinates defined on a sphere-mesh.

we can subsequently orthogonalise vectors (that define our local coordinate system) in the following way:

$$\mathbf{u}_1 = \mathbf{v}_1, \ \mathbf{e}_1 = \frac{\mathbf{u}_1}{\|\mathbf{u}_1\|} \tag{1}$$

$$\mathbf{u}_2 = \mathbf{v}_2 - \mathrm{proj}_{\mathbf{u}_1}(\mathbf{v}_2), \ \mathbf{e}_2 = \frac{\mathbf{u}_2}{\|\mathbf{u}_2\|} \tag{2}$$

$$\mathbf{u}_3 = \mathbf{v}_3 - \mathrm{proj}_{\mathbf{u}_1}(\mathbf{v}_3) - \mathrm{proj}_{\mathbf{u}_2}(\mathbf{v}_3), \ \mathbf{e}_3 = \frac{\mathbf{u}_3}{\|\mathbf{u}_3\|} \tag{3}$$

$$\tag{4}$$

Here $\mathbf{v}_1$, $\mathbf{v}_2$ and $\mathbf{v}_3$ are the initial and possibly not orthogonal guesses of vectors that define our local coordinate system. The vectors $\mathbf{u}_1$, $\mathbf{u}_2$ and $\mathbf{u}_3$ are orthogonalized versions of the vectors $\mathbf{v}_1$, $\mathbf{v}_2$ and $\mathbf{v}_3$. The vectors $\mathbf{e}_1$, $\mathbf{e}_2$ and $\mathbf{e}_3$ are orthonormalized. We employ the Gram-Schmidt orthogonalization to correct initial guesses of the local coordinate system.

3.2.3 Sampling from Appropriate Candidates

For the sampling from the texture image we define a neighborhood template on a regular grid. We obtain the pixel values of the template by projecting the irregular neighborhood vertices onto a flat regular grid that is oriented perpendicular to the surface normal of the currently considered vertex. By doing so, we can apply the same sampling technique that is used in the basic non-parametric sampling approaches. That means one searches for the best candidate pixel values in the example texture and samples from the most likely pixel values. The best candidate pixels are defined by the best locations in terms of the best fitting neighborhood. Employing the described texture generation procedure to a real measurement geometry mesh that is shown in

figure 4 we obtain a textured version of the mesh that is shown in figure 6. The used example texture is a QEMSCAN performed on one of our stone samples. Figure 5 illustrates the vertices of the mesh when the local coordinate system is distributed from one seed onto the whole mesh.

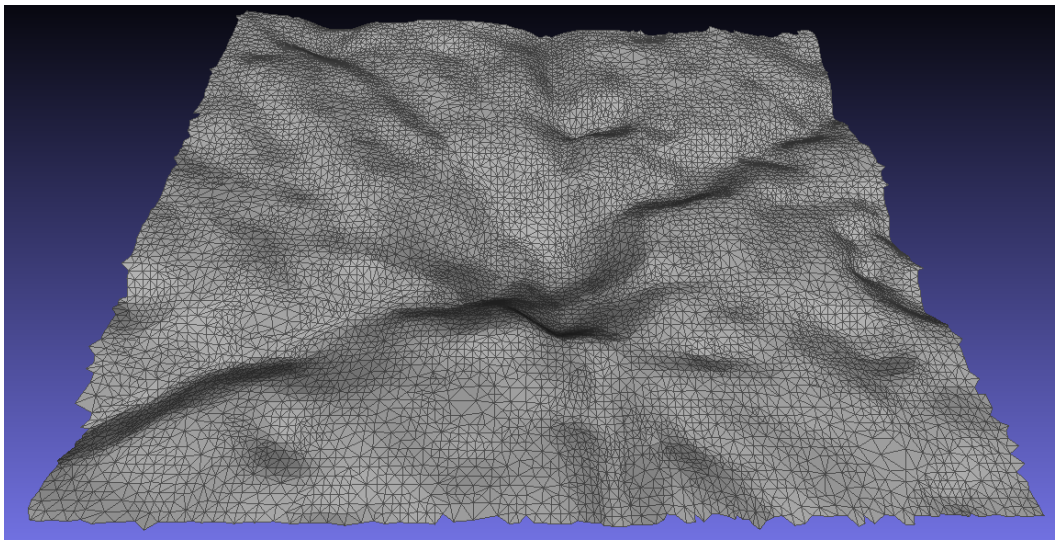

Figure 4: The XMasonMark-part real measurement geometry mesh (Part of the X-Mason-Mark)

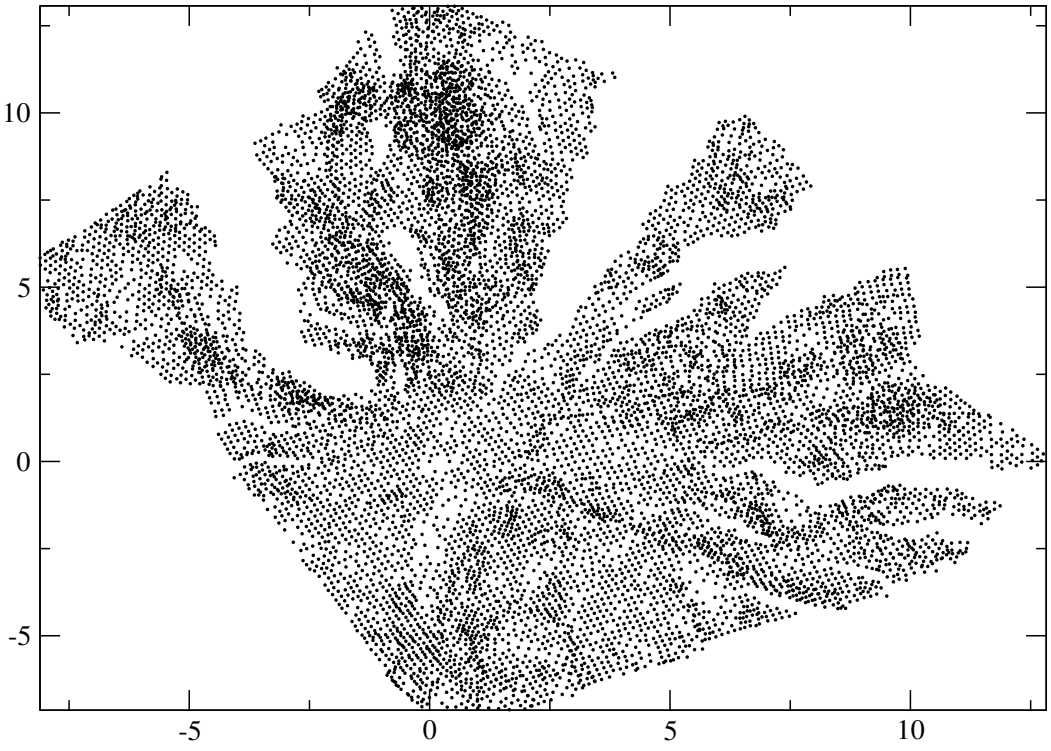

Figure 5: Coordinates of the XMasonMark-part real measurement geometry mesh (Part of the X-Mason-Mark)

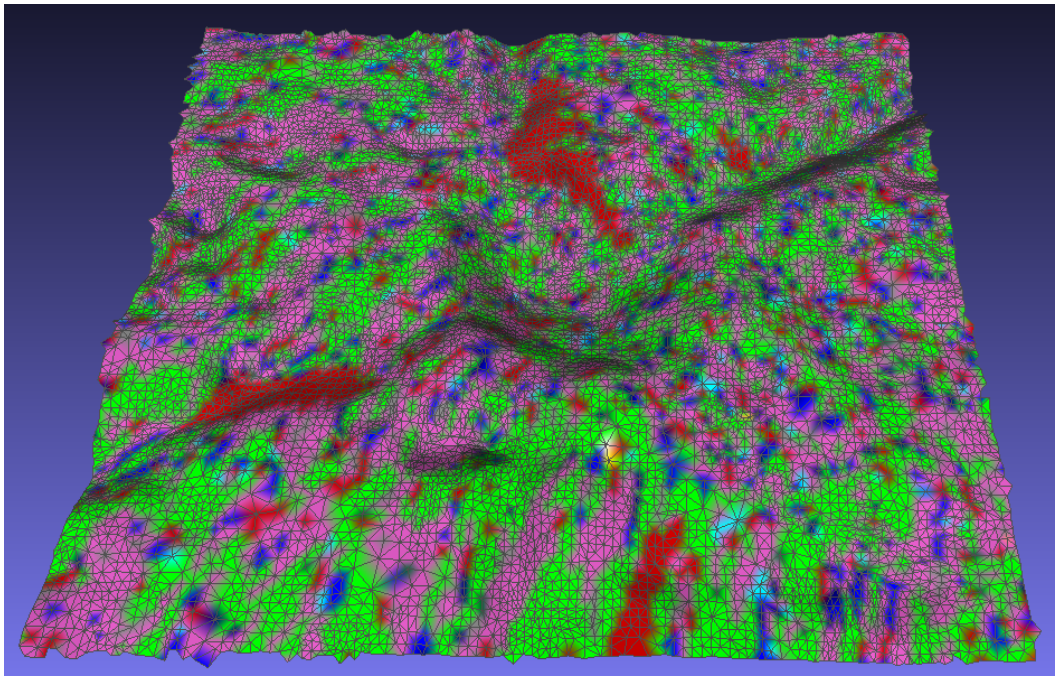

Figure 6: The XMasonMark-part with a sampled mineral map. The result is obtained using the described sampling method and a QEMSCAN measurement as example texture.

4 The Erosion Simulator

4.1 Description of the Erosion Simulator

The purpose of the Erosion Simulator is the simulation of the fundamental and most important degradation mechanisms that impact objects that are made of stone. Therefore the simulator aims to model and simulate the physico-chemical processes that lead to the degradation of the stone-material over time. Towards this aim we implemented a prototype for the mesh alteration that acts on the surface geometry and allows therefore to imitate the surface recession or crust growing. The Erosion Engine implements a mesh off-setting model. This model relies on a computational and a chemical model, which will be subsequently described.

4.2 Modeling Stone Weathering

The main weathering processes responsible for the erosion of rocks and stones are of chemical and physical nature:

Chemical weathering *describes the decay of the stone material into new chemical products by the chemical reactions of the stone material with water and atmospheric gases like carbon dioxide (CO_2), sulfur dioxide (SO_2) and nitrogen dioxide (NO_2).*

Physical or **mechanical weathering** *describes the disintegration of the stone material into smaller particles under the action of heat, water and pressure on the stone, which then can be removed by gravity, wind, water or ice.*

In this current approach we focus on the modeling of the chemical weathering and summarize below the chemical reactions and processes that we consider to be relevant for integration into our stone degradation simulation module.

4.2.1 Chemical Weathering

The two different chemical weathering scenarios that are usually distinguished are the weathering within a **natural environment** and the weathering within a **polluted environment**. The first (unpolluted) scenario considers (beside the air) only the gas carbon dioxide (CO_2) while the second scenario contains also the industrial gases sulfur and nitrogen dioxide (SO_2 and NO_2).

The chemical weathering results in two main effects, the **gain of material** and the **loss of material**. The first one is mostly visible as crust building while the second one relates in most cases to surface recession.

The crust building is usually due to the deposition of chemical material in polluted environments while the loss of material results mainly due to reactions of water with the stone-material and pollution gases. The chemical products of this are subsequently washed away. In the two following paragraphs we refer to the chemical processes that describe the two effects.

Dry deposition in polluted environments The creation of crusts in dry environments is mainly made of gypsum ($CaSO_4 \cdot 2H_2O$) and is the result of reactions of the stone material - calcite ($CaCO_3$) and dolomite ($CaMg(CO_3)_2$) - with the atmospheric gases SO_2 and NO_2. The crust often exfoliates after some time and might result in the removal of a layer of stone. Note that carbonate stones do not react with carbon dioxide CO_2 in dry environments and therefore unpolluted environments do not exhibit crust building.

Recession by acid rain Recession by acid rain is happening both in unpolluted environments due to the gas carbon dioxide (CO_2) and in polluted ones due to the industrial gases sulfur and nitrogen dioxide (SO_2 and NO_2). *Acid rain* contains carbonic acid H_2CO_3, sulfuric acid H_2SO_4 and nitric acid HNO_3 which attack $CaCO_3$ and produce soluble Ca^{2+}, ${HCO_3}^-$ and ${CO_3}^{2-}$ ions. Sulfuric and nitric acid produce the water soluble salts of gypsum $CaSO_4 \cdot 2H_2O$ and nitrocalcite $Ca(NO_3)_2 \cdot 4H_2O$ which drain away as Ca^{2+}, ${SO_4}^{2-}$ and ${NO_3}^-$ ions.

4.3 Modeling Mesh Alteration

The chemical formulas which describe the surface recession provide usually a measure for the change of the surface geometry (deposition/recession δ) of the object surface which depends on the amount of rain fall, stone material and the concentrations of the involved pollution gases. This suggests a simple procedure to simulate erosion acting just on the object surface mesh: For each vertex of the surface mesh one has to calculate the recession rate of the erosion according to the various environmental parameters with adoptions to the local stone material parameters. Then the surface mesh change is performed along the normal direction of the surface.

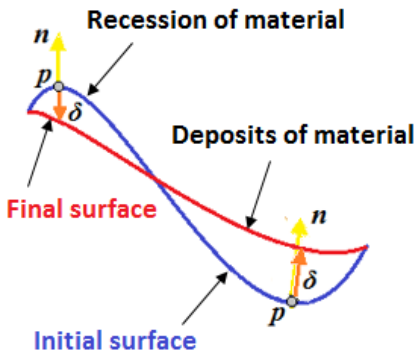

Figure 7: Modeling of an erosion process on the surface of a stone.

4.3.1 Geometric Model of Erosion

Defining the initial surface of a stone as a set of 3D points $S = \{\mathbf{p}_1, \mathbf{p}_2, \ldots, \mathbf{p}_n\}$ and the weathered surface of the same stone in a similar way as $S' = \{\mathbf{p}'_1, \mathbf{p}'_2, \ldots, \mathbf{p}'_n\}$ with $\mathbf{p}_i,\ \mathbf{p}'_j \in \mathbb{R}^3$ one can describe the surface deposition/recession as an offsetting procedure with the help of the diffusion equation.

The diffusion equation

$$\frac{\partial \mathbf{p}}{\partial t} = \mu \nabla^2 \mathbf{p} = \delta \mathbf{n} \ , \tag{5}$$

leads to a simple update rule for computing the offset of the mesh vertices $\mathbf{p}_i$

1. iterate
2. $\mathbf{p}'_i = \mathbf{p}_i + \delta_i \ \mathbf{n}_i \ dt$,
3. until # of epochs (of dt duration each)

Here $\mathbf{n}_i$ is the normal vector at the surface vertex $\mathbf{p}_i$ and δ_i is the surface recession ($\delta_i < 0$) or deposition ($\delta_i > 0$) at this point (see Figure 7). The corresponding

time interval of each epoch is denoted as dt. *Epochs* denote time intervals were different environmental conditions, such as pollution concentration and/or rain fall, can be defined. The number of epochs denotes the total time over which the object is exposed to weathering.

4.3.2 Chemical Model of Erosion

Chemical processes are modeled by the unreacted-core model, which leads to the computation of the mesh offset δ for the following weathering cases [6, 13, 14]:

1. Reaction model for dry deposition of crust due to SO_2

$$\left(\frac{1}{2D_e}\right)\delta^2 + \left(\frac{1}{h_d} + \frac{1}{k_s}\right)\delta = C_{SO_2}\ \frac{M_B}{\rho_B}\ t\ , \tag{6}$$

2. Reaction model for dry deposition of crust due to $SO_2 + NO_2$

$$\left(\frac{1}{2D_{en}}\right)\delta^2 + \left(\frac{1}{k_{sn}}\right)\delta = 2\ a_m\ (C_{SO_2})^{\alpha_1}\ (C_{NO_2})^{\alpha_2}\ \frac{M_B}{\rho_B}\ t\ , \tag{7}$$

3. Reaction model for surface recession by acid rain due to $SO_2 + NO_2 + CO_2$

$$\delta = \left[6.56 + 27.38 \times 10^{(3.0-R_{pH})}\right]\ R_V\ t + 2\ k_r\ (C_{SO_2})^{\alpha_1}\ (C_{NO_2})^{\alpha_2}\ \frac{M_B}{\rho_B}\ t \tag{8}$$

where
δ: the overall crust deposition or the overall surface recession (in cm)
D_e: internal diffusivity (in cm^2/h)
D_{en}: internal diffusivity (in cm^2/h)
h_d: mass transfer coefficient (in cm/h)
k_s: kinetic rate constant (in cm/h)
k_{sn}: kinetic rate constant (in cm/h)
k_r: kinetic rate constant for dry deposition and run-off effect (in cm/h)
M_B: gram-molecular weight of mineral - $M_B = 100.9\ g/mol$ for calcite
ρ_B: density of stone (in g/cm^3) - $\rho_B = 2.714\ g/cm^3$ for marble
a_m: 2.1 (ratio of molar volume of product to reactant)
α_1: 0.7 (relative proportion of sulfate/nitrate)
α_2: 0.3 (relative proportion of sulfate/nitrate)
C_{SO_2}: atmospheric concentration of SO_2 (in mol/cm^3)
C_{NO_2}: atmospheric concentration of NO_2 (in mol/cm^3)
R_V: rain height (in $m/year$)
R_{pH}: rain pH
t: time (in $hours$)

Stone dependent parameters are experimentally calculated in [6, 13, 14]
D_e: $0.14\ cm^2/h$ for marble and $0.37\ cm^2/h$ for dolomite
D_{en}: $0.11\ cm^2/h$ for marble
h_d: $544.27\ cm/h$
k_s: $312\ cm/h$ for marble and $183\ cm/h$ for dolomite
k_{sn}: $375\ cm/h$ for marble
k_r: $2452\ cm/h$ for marble.

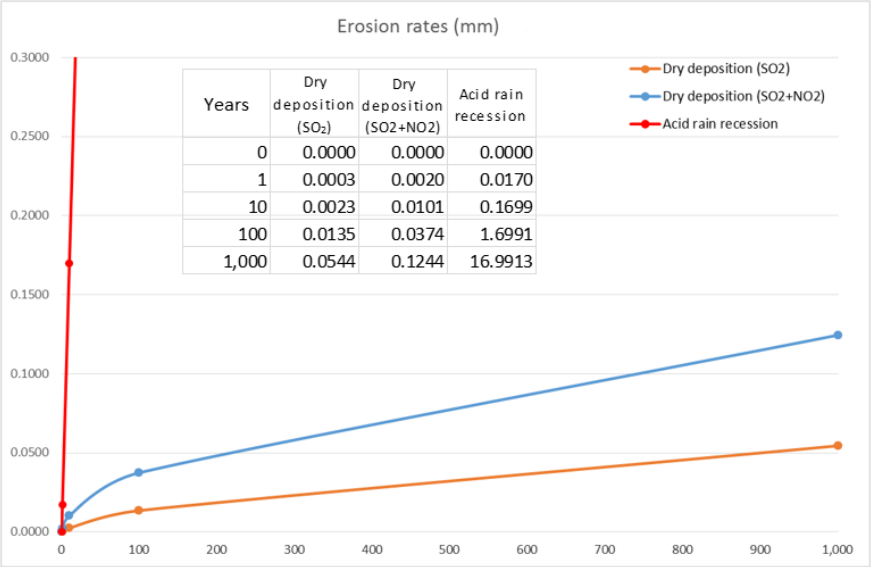

Figure 8: Erosion rates computed on marble under certain environmental conditions for the comparison of the different weathering cases.

An example of the erosion rates (deposition/recession) of marble under certain environmental conditions is depicted in Figure 8, using:
$M_B = 100.9\ g/mol$ (molecular weight of calcite)
$\rho_B = 2.714\ g/cm^3$ (density of marble)
$C_{SO_2} = 4.09 \times 10^{-13}\ mol/cm^3$, for $10\ ppb\ SO_2$ air pollution
$C_{NO_2} = 10.23 \times 10^{-13}\ mol/cm^3$, for $25\ ppb\ NO_2$ air pollution
pH $= 4.5$ for rain acidity
$R_V = 1.13\ m$ rainfall in one year period

Note how dramatically high the recession rates due to acid rain are, compared to the deposition rates of crust in dry environments. This result reaffirms that acid rain recession is the most significant component in the erosion model.

4.4 Erosion Simulator Processing Modes

According to the data types that feed the "Erosion Simulator" module, it can run in two different processing modes.

Surface geometry data The input of the Erosion Simulator is geometric surface data of a known stone type. The Erosion Simulator produces the eroded surface geometry after certain period of time, given a set of stone type and environmental parameters. The output surface is displayed and the erosion effect is measured and rendered.

Surface geometry and surface physico-chemical data The input is physico-chemical data samples over the surface geometry. The surface physico-chemical data for large areas may be synthetically generated from known sample points of certain stone type, by the "Stone Builder" module. The Erosion Simulator produces the eroded surface geometry after certain period of time, given a set of erosion - mineral related - and environmental parameters. The output surface can be displayed and the erosion effect is measured and rendered.

4.4.1 Stone types

The stone types that are going to be modelled are closely related with the stone samples and the experiments carried out in our accelerated erosion chambers for the determination of the physico-chemical parameters of the stones and the reaction models that take place in the degradation process. This modeling is an extension of the Gauri model of erosion which actually works for the simple case of marble that is almost entirely made of calcite.

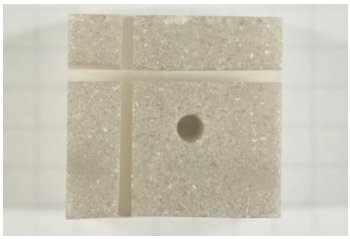

Pentelic Marble:
Elefsis Large 01

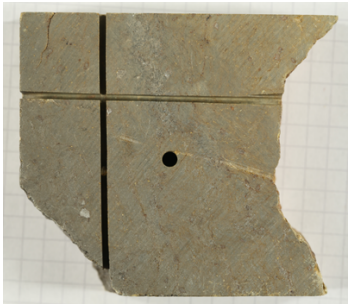

Grytdal Soapstone:
Nidaros Bad Large 01

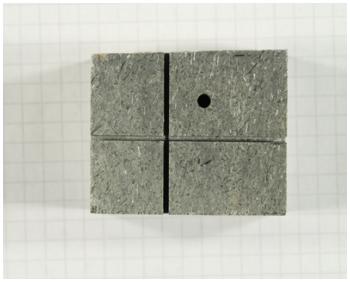

Grytdal Soapstone:
Nidaros Good Large 01

Figure 9: Photos of some stone slabs used in the accelerated erosion experiments.

The experimental samples are stone slabs similar to the stones used at the two Cultural Heritage sites; the Demeter Sanctuary in Elefsis, Greece, and the Nidaros Cathedral in Trondheim, Norway. Pentelic marble was used at the Demeter Sanctuary [7] and Grytdal soapstone was used in the Nidaros Cathedral [11]. The stone slabs were named according to their origin (Elefsis, Nidaros); furthermore the soapstone slabs labelled with reference to the stone quality (Good, Bad) and finally according to their size (Large, Small) (see Figure 9).

The stone types under experimental study in our accelerated erosion chambers are:

Pentelic Marble Dense metamorphic rock; homogeneous; almost entirely made of calcite ($96\%\ CaCO_3$); with low porosity ($3.64\ vol\%$) [7].

Grytdal Soapstone Dense metamorphic rock; non homogeneous; made mostly of chlorite ($20\% - 60\%$) and talc ($5\% - 20\%$); with low porosity ($3.60\ vol\%$) [11].

4.4.2 Data modalities

The input of the Erosion Simulator is geometric surface data and surface physico-chemical data. The data sets currently used as input data of the Erosion Simulator are summarized below:

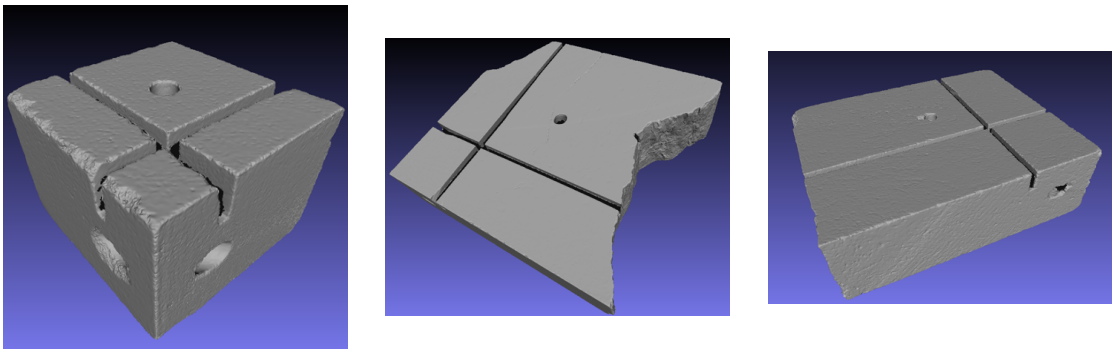

Pentelic Marble: Elefsis Large 02 | Grytdal Soapstone: Nidaros Bad Large 02 | Grytdal Soapstone: Nidaros Good Large 02

Figure 10: Depiction of the 3D scans of some stone slabs.

3D Geometry Scans The 3D scans of the stone slabs in high resolution surface meshes of the 3D geometry of the stones, were performed by Aicon – our industrial partner in the PRESIOUS project – using a Breuckmann Scanner [1]. Examples of the resulting mesh data are depicted in Figures 10 and 16.

QEMSCAN Quantitative Evaluation of Minerals by SCANning electron microscopy is a technique that uses a Scanning Electron Microscope (SEM) combined with X-ray spectroscopy and a database to obtain accurate mineral maps for a measured stone surface, performed by Robertson CGG [10]. The results of the QEMSCAN of some of the stone slabs are shown in Figures 11 (a) and (b). The used color codes and labeling of the mineral map is shown in Figure 11 (c).

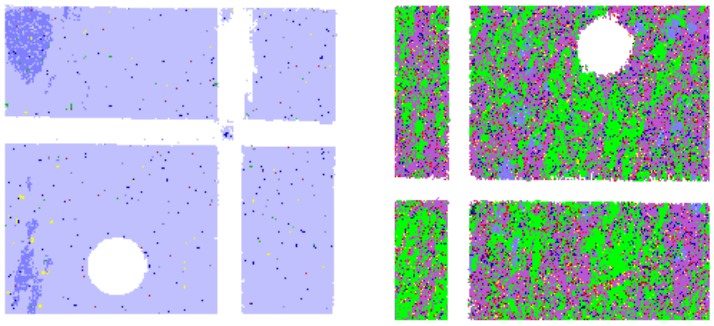

Minerals	Color	RGB-dec		
Quartz		255	255	0
K-Feldspar		221	160	221
Plagioclase Feldspar		255	105	180
Biotite		128	0	0
Illite		0	192	0
Chlorite		0	255	0
Smectite		51	102	0
Kaolinite		192	64	0
Glauconite		128	128	0
Calcite		192	192	255
Dolomite		128	128	255
Ankerite		255	192	128
Siderite		255	128	0
Gypsum/Anhydrite		178	34	34
Pyrite		255	215	0
Heavy Minerals		255	0	0
Altered Mafics		186	85	211
Pores		0	0	192
Others		128	128	128
No measurement		255	255	255

(a) Pentelic Marble: Elefsis Large 01

(b) Grytdal Soapstone: Nidaros Good Large 01

(c) Color codes of the QEMSCAN minerals

Figure 11: Depiction of the mineral maps from the QEMSCAN of some stone slabs.

4.4.3 Application of the Erosion Simulator on a mesh of homogeneous stone

In this first mode, the input of the Erosion Simulator is 3D geometric surface data only, in a mesh structure. The Erosion Simulator considers that data come from a homogeneous stone of a known type. The Erosion Simulator produces the eroded surface geometry considering that δ for deposition/recession *is the same on every vertex of the mesh*, determined by the stone type and the environmental parameters.

In this mode, the simulator runs on various complete irregular or regular meshes acquired at different resolutions with mean-edge-length at $0.060 \sim 0.098\ mm$ (see Figures 18 and 19).

For example the implementation of this fundamental surface offsetting model is applied to the surface mesh of the Elefsis pillar. The effect of this thinning process is depicted in Figure 12. The result simulates the acid rain recession on marble, under certain environmental conditions over a period of 200 years, yielding a surface offset of almost $3.4\ mm$.

4.4.4 Application of the Erosion Simulator on a mesh textured with a mineral map

In this second mode, the input of the Erosion Simulator involves geometric information in the form of a mesh and mineral data assigned on the surface of the object being eroded. The surface physico-chemical data for large areas - such as the Elefsis Pillar or the Nidaros Cathedral walls - may be synthetically generated from known stone mineral maps, by the "Stone Builder" module. The surface physico-chemical

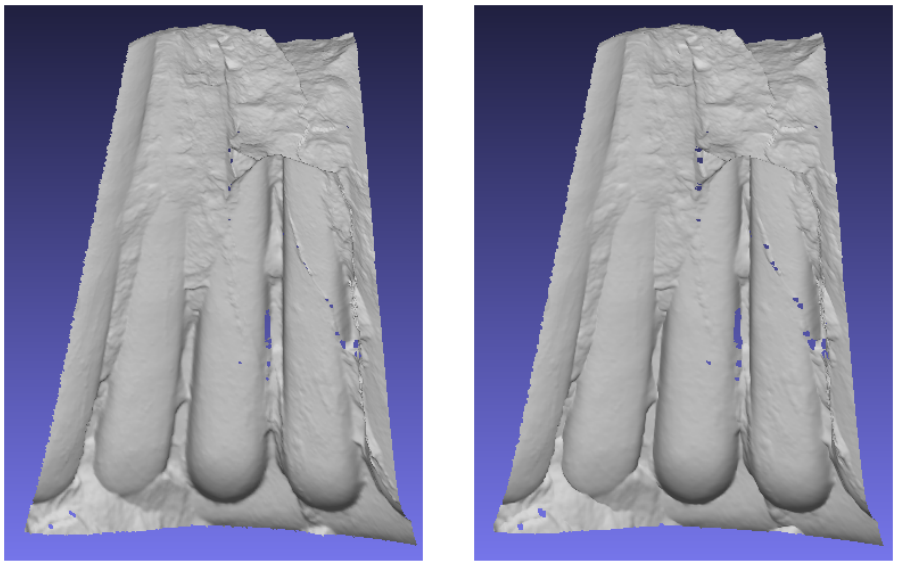

(a) **(b)**

Figure 12: Modeling of an erosion process on the surface of Elefsis pillar: (a) original stone surface; and (b) weathered (thinned) stone surface due to acid rain recession over a period of 200 years.

data of the stone slabs can be created by registering the available 3D scanned meshes and the QEMSCAN texture information. The Erosion Simulator produces the eroded surface geometry considering that δ for deposition/recession *is different on every vertex of the mesh*, and is determined by the mineral type assigned to it and the environmental parameters. δ dependencies on mineral attributes have to be determined by experimental data.

A crucial first step for this procedure is the registration of the acquired geometric mesh data with the QEMSCAN mineral map texture data (Figures 20 and 21). The general registration transformation matches landmark points annotated on the geometry image of the scanned 3D mesh, and the corresponding landmark points annotated on the QEMSCAN texture, which are considered as the invariant reference points under the correspondence transformation. These points are localized using the hole and the cross which are engraved onto the slabs for this purpose (see Appendix B).

In this mode, the simulator runs on various regular meshes re-sampled at different resolutions with mean-edge-length at $0.035 \sim 0.050\ mm$ textured with QEMSCAN mineral map images (see Appendix A).

Although the Erosion Simulator is currently in a version which can deal with the combination of geometric mesh data along with registered mineral map texture, the physico-chemical model that drives this per-mineral erosion computation is not completed yet.

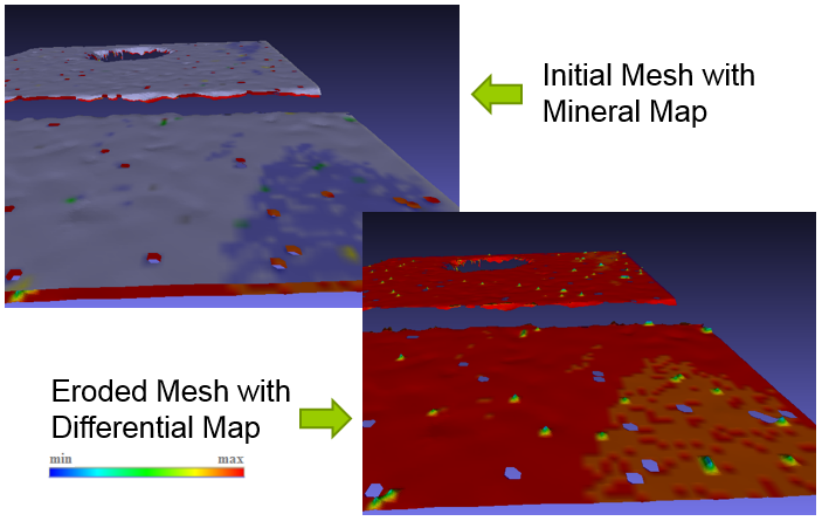

Figure 13: Erosion prediction for the Elefsis Large 1 (EL1) slab (red indicates most eroded areas and blue least eroded areas).

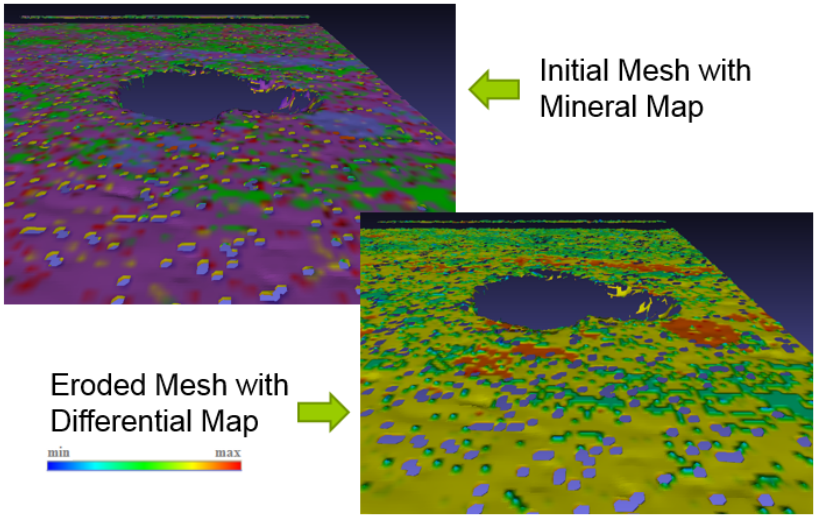

Figure 14: Erosion prediction for the Nidaros Good Large 2 (NGL2) slab (red indicates most eroded areas and blue least eroded areas).

The predictions of the Erosion Simulator are depicted in Figures 13 and 14 for viewing purposes only, by just applying a different offset values at vertices having different mineral composition according to the conjecture that some minerals will be eroded more and some less. This is done by enhancing for other minerals the Gauri model for $CaCO_3$ by using a simple analogy

$$\delta(other) = \alpha(other)\ \delta(CaCO_3)$$

Parameter α has for the moment arbitrary values that have to be determined and evaluated by analysing the results of the accelerated erosion experiments and the on-site erosion measurements.

4.5 Erosion prediction complexity and running times

Table 1: Comparison of the proposed erosion computation running times for one epoch over Elefsis Large 3 (EL3) and Elefsis Small 1 (ES1) slabs: (a) on the regularly resampled frontal area; and (b) on the whole scanned irregular mesh

Running times			
Stone	facets	vertices	t (sec)
$\mathbf{EL3}^{(a)}$	295,643	149,451	3.01
$\mathbf{EL3}^{(b)}$	1,960,187	983,698	18.38
$\mathbf{ES1}^{(a)}$	278,244	140,690	2.77
$\mathbf{ES1}^{(b)}$	1,296,290	652,069	12.18

The complexity of the current version of the Erosion Simulator is linear in the number of vertices of the mesh being eroded. Some typical running times on an Alienware computer (Intel Core i7 @ 3.6 GHz, 16 GB RAM) are given in Table 1.

The current version of the Erosion Simulator is therefore near real-time for relatively small meshes, allowing the user to experiment with various scenaria.

5 The Differential Measurer

5.1 Description of the Differential Geometry Measurer

The Differential Geometry Measurer is the component within our "Object Degradation Prediction" module that measures the erosion of stone surface areas that are scanned consecutively within this workpackage at the cultural heritage sites (or alternatively using stone slabs exposed to accelerated erosion). Therefore one has to perform first an accurate surface registration followed by the actual measurement of the erosion effects that appear on the cultural heritage objects over time.

A key problem in measuring erosion based on scans made across time is the difficulty in registering these scans. Due to the absence of an external reference frame, a typical registration algorithm, such as Iterative Closest Point (ICP) [2], aligns the scans so as to minimize the RMS error between them, which is not an ideal solution in case of large erosion, since it diminishes the common erosion that has to be measured. However, if most of the eroded surface is unaltered this method might be sucessfully applied for registration.

In order to obtain an accurate surface registration of two surfaces that show a different degree of erosion we pursued the goal to exploit and extend existing techniques that allow the estimation of an optimal transformation between the two surfaces such that their shapes match as closely as possible.

5.2 Stone Surface Registration

For surfaces where the erosion appears only as local loss of material Iterative Closest Point (ICP) algorithms are still a suitable joice as one expects the optimal registration to coincide with the desired registration. This is for example the case for the surface measurements of the real stone monuments we investigate. For our purposes any tool that registers the surfaces with for example ICP (like the commercial Windows software OPTOCAT from Breuckmann/Aicon) is a suitable tool for registering and aligning the slightly eroded stone surface areas. The mesh differences can then be computed using the Differential Geometry Measurer tool.

For the stone slabs for which we expected a large recession of the surface area we investigate techniques for registering the surfaces that are based on identifying and aligning cylindrical holes that were drilled into the stones prior to the erosion experiments. The stones were measured with volumetric X-Ray scans and with high accurate surface scanning. For registering the surface data we currently follow an idea to use the surface-normals within an adapted 3D Hough transform (Using the 3D space as accumulator space for the surface-normals) to identify and register the axis of the cylindrical holes. In addition we develop a method for registering the large three dimensional X-ray CT scans of the stone slabs. This is performed in two phases: First a rough registration on downscaled versions of the volumes are used to obtain an initial alignment by exploiting a Phase correlation of the Fourier transforms of the stone volume data. In the second phase the initial registration is improved by a gradient descent strategy.

5.3 Computing erosion on the stone mesh

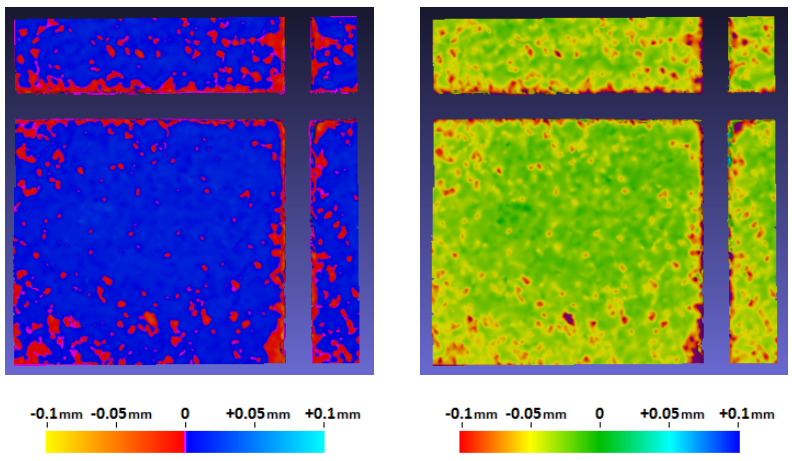

Figure 15: Differential Maps of initial to eroded mesh for the frontal surface of the stone slab Elefsis Large 3 (EL3) using two different color maps (a) and (b) both in the interval of $[-0.1\ mm \sim +0.1\ mm]$.

Consider two point sets $M = \{\mathbf{m}_1, \mathbf{m}_2, \ldots, \mathbf{m}_p\}$, that represents the initial surface of a stone, and $T = \{\mathbf{t}_1, \mathbf{t}_2, \ldots, \mathbf{t}_q\}$ that represents the weathered surface of the same stone, where $\mathbf{m}_i,\ \mathbf{t}_j \in \mathbb{R}^3$.

The average directed Hausdorff distance $D_{MH}(M,T) = \frac{1}{p}\sum_{i=1}^{p} \min_j(\|\mathbf{m}_i - \mathbf{t}_j\|$ is used as an overall mean erosion measure for the whole stone or a portion of it (see Appendix C).

The distance $d_e(\mathbf{m}_i) = \min_j(\|\mathbf{m}_i - \mathbf{t}_j\|)$ is used as a local erosion measure which expresses at each vertex of the initial model M the distance of the closest vertex of the eroded model T, and is a scalar mapping of the erosion measure at each vertex of the initial stone model M, to which the eroded model T is registered. $\|\mathbf{m}_i - \mathbf{t}_j\|$ is the Euclidean distance of a point of M from a point of T.

Figure 15 depicts the distance maps (i.e. the $d_e(\mathbf{m}_i)$) between round 01 and 02 meshes of Elefsis Large 3, and consequently the computed erosion measure textured on the initial mesh.

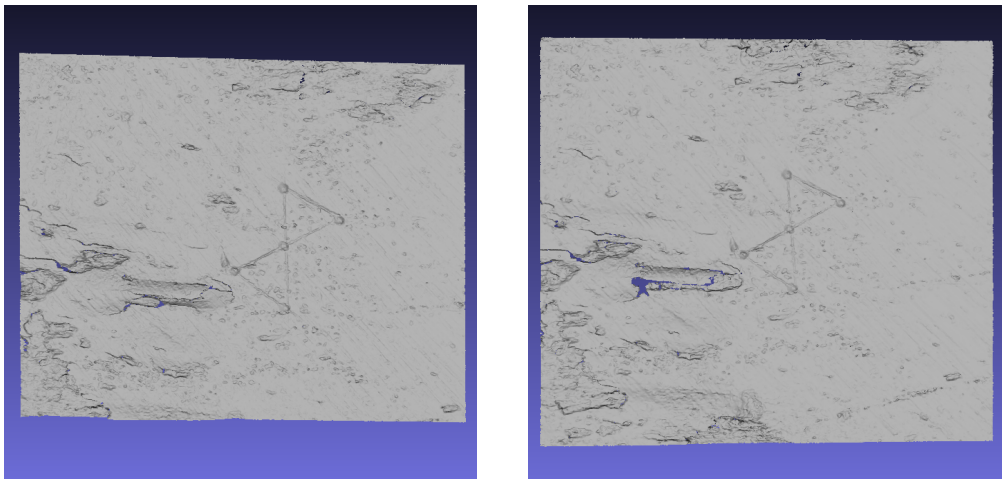

X mason mark
(Round 01, 2013-04-10)

X mason mark
(Round 02, 2014-09-24)

Figure 16: Patches of two geometric measurement rounds showing the X mason mark that are present on the east wall of the Lectorium of the Nidaros Cathedral.

At Nidaros Cathedral several areas were selected for scanning. These include two wall parts from the Lectorium (Lectorium East, with Mason Marks, and Lectorium North) and two scans from the inside of the North West and South West Tower of the Cathedral. Figures 16 depict a close-up view of the geometric scans of the east wall of the Lectorium of Nidaros Cathedral that contains two mason marks. Figure 17 depicts the distance map of the two X mason mark patches between the two Round 01 and Round 02 scanning periods, and consequently the experimental erosion measure mapped on the initial mesh.

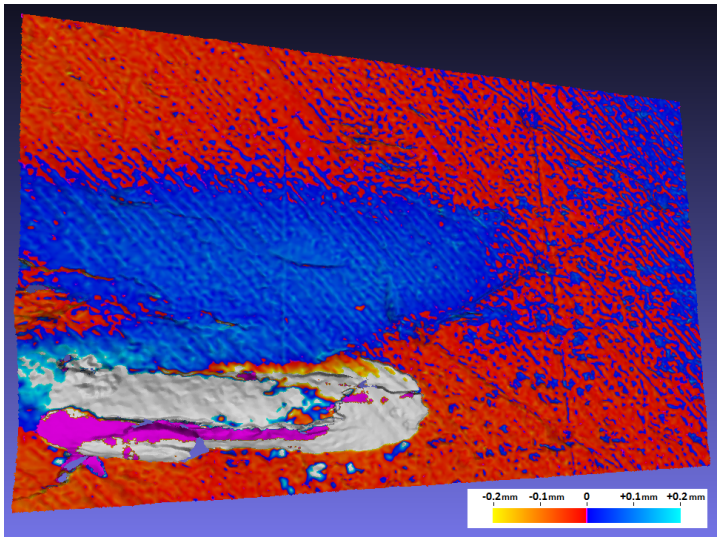

Figure 17: Distance map of the two X mason mark patches between the two Round 01 and Round 02 3D geometry acquisitions. The meshes are at first registered, and then distances are mapped as textures onto the Round 01 mesh.

6 Concluding remarks

This report describes the design and implementation of a prototype software application that simulates surface mesh alterations of Cultural Heritage objects and allows therefore to imitate manifestations of stone degradation phenomena like surface recession and crust formation. However, a simulation of this type proved to be extremely challenging, both because of the large number of parameters involved and because of the difficulty involved in bench-marking these parameters with actual experimental data values. Simulating all the natural effects that contribute to erosion is rather chaotic and also a long term process, thus we tried to focus on the most important effects and tried to simulate these experimentally in isolation for the specific stone types that were used in the two Cultural Heritage sites we are studying, i.e. Pentelic marble and two types of Grytdal soapstone. Also, for the purpose of determining in reasonable time the degradation phenomena parameters that drive the erosion simulation, erosion chambers were built and stone samples were exposed to accelerated erosion.

Although the implementation of the "Degradation Prediction" module has substantially improved, there are still some unsolved issues that most of the module components suffer. These mostly come from the fact that the interpretation of the results from the accelerated weathering experiments on the marble and soapstone at macroscopic and microscopic levels is still in progress, and although we can infer that the investigation conducted has given an insight into the changes occurring during erosion/weathering of these stones, the difficulties for incorporating these qualitative results in a quantitative simulation model still remain.

Some of the challenges we faced are the following:

- ICP registration is not sufficient. By minimising the overall registration error, it "misses" the possible erosion "common" to all points. For this reason, it may be only possible to measure relative rather than absolute erosion values since there are no external fixed reference points.
- ICP is not efficient for large data sets, such as that acquired from Nidaros and Elefsis, because it has quadratic complexity, even if the data is split in an octree data structure.
- The Gauri erosion model, which has been implemented in the Erosion Simulator, is only applicable to calcium carbonate stones exposed to acid rain polluted by SO_2 and NO_2.
- The Nidaros slabs exhibited an unexpected swallowing behaviour in both acid solution chambers; this has not yet been interpreted or modelled.
- The per-mineral recession rates of the stones exposed in the chemical erosion chambers seem quite chaotic and difficult to related to the experimental parameters of the erosion chambers.
- The environmental parameters of the Gauri model have not yet been related to the chemical parameters of the acid solution erosion chambers.

A Geometric data resampling

Surfaces can be represented by a global bijective parameterization of the form

$$\mathbf{p}(u,v) = [x(u,v), y(u,v), z(u,v)]^T \ , \tag{9}$$

where (u,v) are coordinates on the parameterization domain, usually on the unit square $(u,v) \in [0,1] \times [0,1]$.

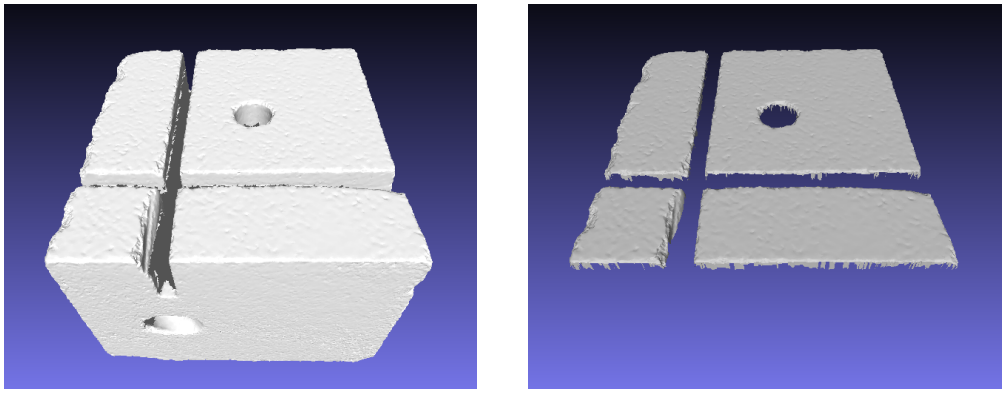

(a) (b)

Figure 18: Depiction of mesh of the stone slab Elefsis Large 1 (EL1): (a) the complete scanned irregular mesh (mean-edge-length at $0.060 \sim 0.098\ mm$); and (b) the regularly resampled frontal area (mean-edge-length at $0.035 \sim 0.050\ mm$).

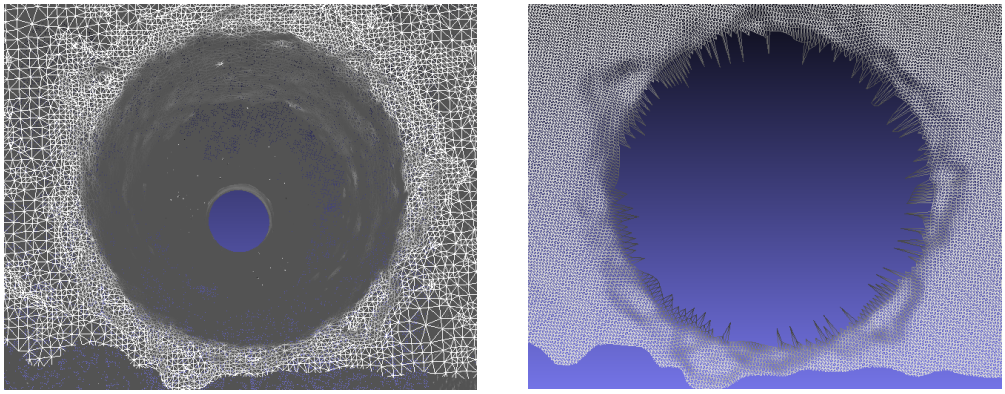

(a) (b)

Figure 19: Detail of the mesh of the stone slab Elefsis Large 1 (EL1) near the hole area: (a) the scanned initial irregular mesh; and (b) the regularly resampled area.

Sampling of surface properties in their preimage (bijective parametric domain or *Texture Atlas*) is convenient because the neighborhood of a point under consideration is known and texture information can easily be assigned to it. We can sample a surface in a uniform way on the parameterization domain and create a Cartesian grid of values, which can be stored in matrix form, and displayed as a bitmap image (i.e. a *Geometry Image*). This way 2D maps of the 3D information of a surface can be stored and subsequently processed [9].

Algorithm 1 "Regular Orthographic Mesh Sampling" [9]

Require: Surface mesh (V, F) and texture image $I(u, v)$, $u_{samples}$, $v_{samples}$.
Ensure: Geometry image I_G and texture image I_T.

Compute surface bounding box $(x_{min}, x_{max}, y_{min}, y_{max}, z_{min}, z_{max})$.
$u_{step} := (x_{max} - x_{min})/u_{samples}$.
$v_{step} := (y_{max} - y_{min})/v_{samples}$.
for $i := 1 \ldots u_{samples}$ **do**
    $x := x_{min} + (i - 1) * u_{step}$.
    for $j := 1 \ldots v_{samples}$ **do**
        $y := y_{min} + (j - 1) * v_{step}$.
        Consider line $(\mathbf{p}_0, \mathbf{p}_1)$ with $\mathbf{p}_0(x, y, z_{min})$ and $\mathbf{p}_1(x, y, z_{max})$.
        for $f := 1 \ldots \#facets$ **do**
            Get facet vertices $(\mathbf{v}_0, \mathbf{v}_1, \mathbf{v}_2)$.
            Compute line-facet intersection point $\mathbf{q}(x, y, z)$.
            if (intersection) **then**
                Compute texture coordinates (u, v) that correspond to $\mathbf{q}(x, y, z)$.
                Get texture value $I(u, v)$ using bilinear interpolation.
                BREAK
            end if
        end for
        if (intersection) **then**
            $I_G(i, j) := \mathbf{q}(x, y, z)$.
            $I_T(i, j) := I(u, v)$.
        end if
    end for
end for
return I_G and I_T.

For creating a regular (u, v) parametric surface we utilize an orthographic regular resampling of the 3D irregular surface mesh (see Algorithm 1). The resulting surface is able to represent the curved surface of a stone as accurately as required for our purposes (mean-edge-length at $0.035 \sim 0.050\ mm$), i.e. dense enough for registering QEMSCAN data as texture information (Figures 18 and 19)

By subsequently registering the texture image (i.e. the QEMSCAN image), a unified representation of 3D and 2D data is accomplished by a (u, v) parametric map. Thus the 3D and 2D information can be cross-referenced (Figure 22(g)).

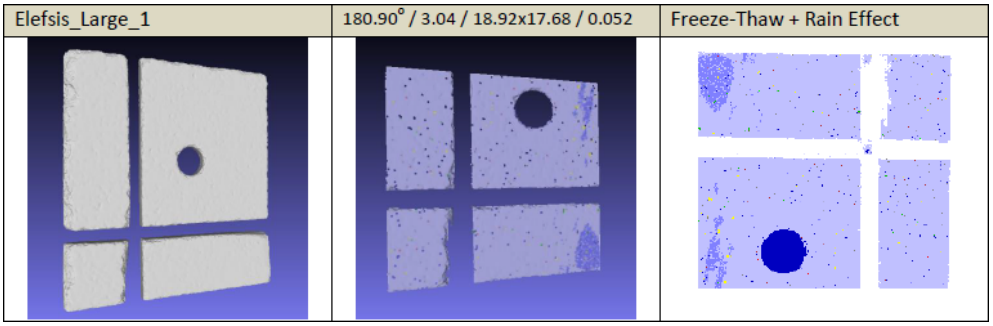

Figure 20: Depiction of geometry and QEMSCAN registration results for the Elefsis Large 1 (EL1) marble slab.

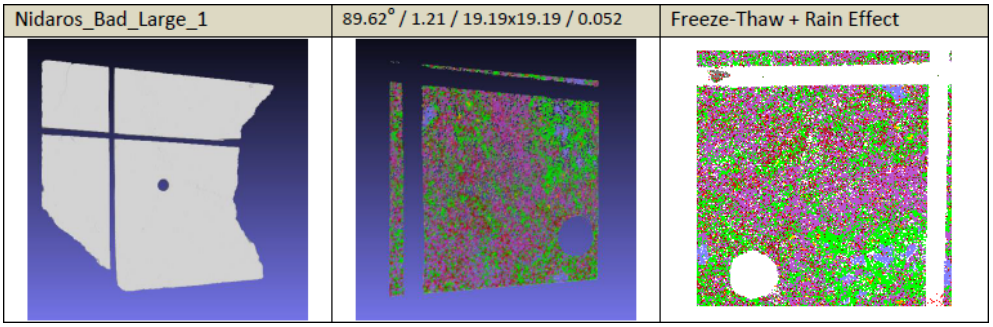

Figure 21: Depiction of geometry and QEMSCAN registration results for the Nidaros Bad Large 1 (NBL1) soapstone slab.

Results of the regular sampling and texture registration procedure for the "Elefsis Large 1" and the "Nidaros Bad Large 1" stone slabs are depicted in Figures 20 and 21.

B Registration of geometric and mineral data

The registration procedure between the geometric mesh and the mineral map texture is depicted in Figure 22. Every point (pixel) $\mathbf{p}_1$ on the texture image (Fig. 22(d)) has a corresponding point $\mathbf{p}_0$ on the geometry image (Fig. 22(c)), from where we can get the 3D coordinates of it, using bilinear interpolation, since generally it will

not coincide with a pixel on the geometry image after applying the correspondence transformation. Thus, a 3D surface patch with registered texture (Fig. 22(g)) is created.

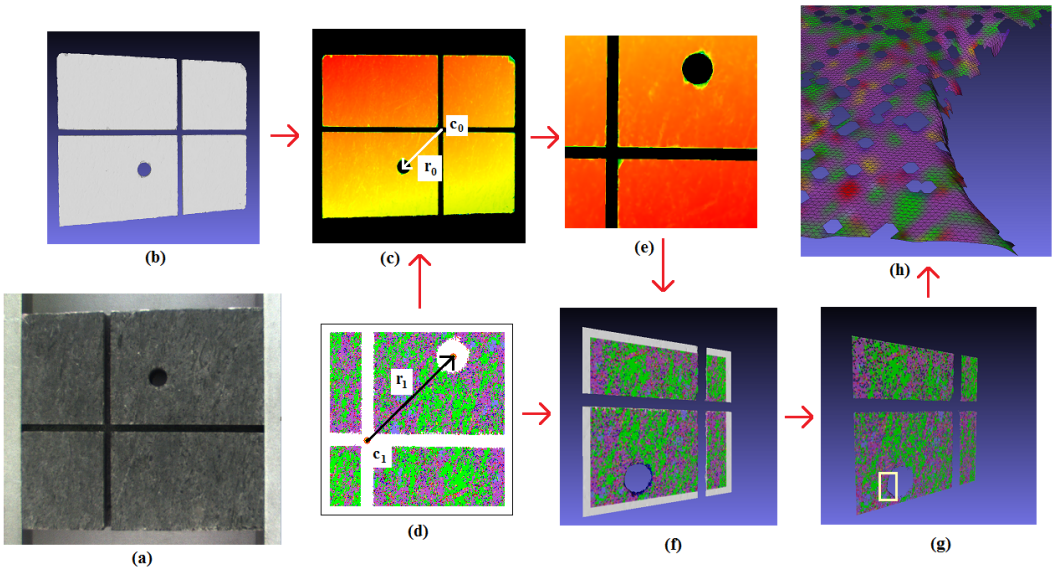

Figure 22: Depiction of the registration procedure of Nidaros Good Large 1 (NGL1): (a) Stone photo; (b) Mesh data regularly re-sampled; (c) Geometry image (depicted as depth image) of regular surface mesh; (d) Mineral map; (e) Depth image of mineral map after registration; (f) Surface mesh with registered mineral map as texture; (g) Cleaned mesh (w/o white space and pores); (h) Detail of mesh and texture.

Case 1: Two corresponding point pairs are given Points, $\mathbf{c}_0$ and $\mathbf{c}_1$, are considered the invariant reference points under the correspondence transformation, and $\mathbf{r}_0$ and $\mathbf{r}_1$ are the vectors defined by two other corresponding known points. These two pairs of points are annotated landmark points on the two images. Thus, the following transformations solve this problem of correspondence [9]:

$$\mathbf{p}_0 - \mathbf{c}_0 = \mathbf{M}_z(\mathbf{p}_1 - \mathbf{c}_1)$$

with

$$\mathbf{M}_z = \begin{bmatrix} a & -b \\ b & a \end{bmatrix}$$

where

$$\phi_z = tan^{-1}\left(\frac{b}{a}\right)$$

is a rotation around $\mathbf{z}$ (the normal to the image plane), and

$$s = \sqrt{a^2 + b^2}$$

is a scaling.

Parameters, a and b, are calculated according to:

$$a = (r_{0x}r_{1x} + r_{0y}r_{1y})/(r_{1x}^2 + r_{1y}^2)$$

and

$$b = (r_{0y}r_{1x} - r_{0x}r_{1y})/(r_{1x}^2 + r_{1y}^2) \ .$$

Case 2: A pair of corresponding points and a pair of corresponding directions are given Points, $\mathbf{c}_0$ and $\mathbf{c}_1$, are considered the invariant reference landmark points under the correspondence transformation, and $\mathbf{r}_0$ and $\mathbf{r}_1$ are the vectors defined by two other known landmark points. In this case $\mathbf{r}_0$ and $\mathbf{r}_1$ define just two corresponding directions in the two images. Points, $\mathbf{c}_0$ and $\mathbf{c}_1$, are the only corresponding points on each image. The following transformations solve this problem of correspondence [9]:

$$\mathbf{p}_0 - \mathbf{c}_0 = \mathbf{M}_z(\mathbf{p}_1 - \mathbf{c}_1)$$

with

$$\mathbf{M}_z = \begin{bmatrix} a & -b \\ b & a \end{bmatrix}$$

which can be separated into a rotation and a scaling

$$\mathbf{M}_z = \begin{bmatrix} cos\phi & -sin\phi \\ sin\phi & cos\phi \end{bmatrix} s$$

with

$$cos\phi = a/(a^2 + b^2)$$

and

$$sin\phi = b/(a^2 + b^2) \ .$$

Parameters, a and b, are calculated according to:

$$a = (r_{0x}r_{1x} + r_{0y}r_{1y})/(r_{1x}^2 + r_{1y}^2)$$

and

$$b = (r_{0y}r_{1x} - r_{0x}r_{1y})/(r_{1x}^2 + r_{1y}^2) \ .$$

Finally, s can be determined by the length-metric (inter-pixel distance) of each image, m_0 and m_1,

$$s = m_1/m_0$$

Length-metric m_0 is computed from the geometry image. Length-metric m_1 for the mineral map image is computed from available data ($m_1 = 91\mu m/pixel$).

Remarks: In the case of two landmark points the above correspondence transformations solve exactly the registration problem and the solution exactly matches the two pairs of landmark points. In the case of more than two landmark points the problem is over-determined, and these transformations (properly generalized) minimize the MSE between the calculated landmarks from the transformations and the annotated ground-truth landmarks [9].

C Hausdorff distance as a metric of stone erosion

Consider two point sets:

$$M = \{\mathbf{m}_1, \mathbf{m}_2, \ldots, \mathbf{m}_p\}$$

that represents the initial surface of a stone, and

$$T = \{\mathbf{t}_1, \mathbf{t}_2, \ldots, \mathbf{t}_q\}$$

that represents the weathered surface of the same stone, where $\mathbf{m}_i,\ \mathbf{t}_j \in \mathbb{R}^3$.

The *standard Hausdorff* distance is defined as:

$$D_H(M,T) = \max(D_h(M,T), D_h(T,M)) \ ,$$

where

$$D_h(M,T) = \max_i(\min_j(\|\mathbf{m}_i - \mathbf{t}_j\|)) \ ,$$

is the *directed Hausdorff* distance from M to T.

The directed Hausdorff distance expresses the Euclidean distance $\|\mathbf{m}_i - \mathbf{t}_j\|$ of the farthest point of M from any point of T, i.e., the maximum value of the minimum Euclidean distances of the points of M from any point of T.

The *average directed Hausdorff distance* D_{MH}, of an initial stone model M to an eroded stone model T, can be defined [5, 9], as:

$$D_{MH}(M,T) = \frac{1}{p}\sum_{i=1}^{p} \min_j(\|\mathbf{m}_i - \mathbf{t}_j\| \ , \tag{10}$$

where $\|\mathbf{m}_i - \mathbf{t}_j\|$ is the Euclidian distance between the initial model vertices $\mathbf{m}_i$ and the eroded model vertices $\mathbf{t}_j$, and p the number of the model vertices. D_{MH} expresses the mean value of the minimum Euclidean distances $\|\mathbf{m}_i - \mathbf{t}_j\|$ of the points of M from any point of T.

The average directed Hausdorff distance D_{MH} can be used as an overall mean erosion measure for the whole stone or a portion of it.

The distance $d_e(\mathbf{m}_i) = \min_j(\|\mathbf{m}_i - \mathbf{t}_j\|)$ can be used as a local erosion measure which expresses at each vertex of the initial model M the distance of the closest vertex of the eroded model T, and is a scalar mapping of the erosion measure at each vertex of the initial stone model M, to which the eroded model T is registered.

References

[1] AICON 3D systems, *http://aicon3d.com/start.html*, 2015.

[2] Paul J. Besl and Neil D. McKay, *A method for registration of 3-D shapes*, IEEE Trans. Pattern Anal. Mach. Intell. **14** (1992), no. 2, 239–256.

[3] Eric Doehne and Clifford A. Price, *Stone conservation: An overview of current research*, Technical report, Los Angeles, 2010.

[4] Alexei Efros and Thomas Leung, *Texture synthesis by non-parametric sampling*, In International Conference on Computer Vision, 1999, pp. 1033–1038.

[5] Y. Gao, *Efficiently comparing face images using a modified Hausdorff distance*, Proc. IEEE Conference on Vision, Image and Signal Processing, Dec. 2003, pp. 346–350.

[6] K. Lal Gauri and J. K. Bandyopadhyay, *Carbonate stone, chemical behaviour, durability and conservation*, John Wiley & Sons, Inc., 1999.

[7] A. Moropoulou, K. Bisbikou, K. Torfs, R. van Grieken, F. Zezza, and F. Macri, *Origin and growth of weathering crusts on ancient marbles in industrial atmosphere*, Atmospheric Environment **32** (1998), no. 6, 967–982.

[8] Rupert Paget, *Nonparametric markov random field models for natural texture images*, Ph.D. thesis, University of Queensland, 1999.

[9] Panagiotis B. Perakis, *Landmark Detection for Unconstrained Face Recognition*, Ph.D. thesis, Dept. of Informatics and Telecoms, University of Athens, July 2013.

[10] Robertson CGG, *http://www.robertson-cgg.com/*, 2015.

[11] Per Storemyr, *The stones of nidaros: an applied weathering study of europe's northernmost medieval cathedral*, Ph.D. thesis, Norwegian University of Science and Technology (NTNU), 1997.

[12] Li-Yi Wei and Marc Levoy, *Texture synthesis over arbitrary manifold surfaces*, Proceedings of the 28th Annual Conference on Computer Graphics and Interactive Techniques (New York, NY, USA), SIGGRAPH '01, ACM, 2001, pp. 355–360.

[13] S. Yerrapragada, S. Chirra, J. Jaynes, S. Li, J. Bandyopadhyay, and K. Gauri, *Weathering rates of marble in laboratory and outdoor conditions*, Journal of Environmental Engineering **122** (1996), no. 9, 856–863.

[14] Srinivas S. Yerrapragada, John H. Jaynes, Surendra R. Chirra, and K. L. Gauri, *Rate of weathering of marble due to dry deposition of ambient sulfur and nitrogen dioxides*, Analytical Chemistry **66** (1994), no. 5, 655–659.